Biomaterials Science

PAPER

View Article Online
View Journal | View Issue

Check for updates

Cite this: *Biomater. Sci.*, 2025, **13**, 6805

# Rapid and label-free isolation of human peripheral blood monocytes using a reversible CD36-binding aptamer for cell capture

Melissa Ling,[a] Nataly Kacherovsky,[b] Abe Y. Wu,[b] Minjian Ni,[c] Jessica A. Hamerman[c] and Suzie H. Pun *[a,b]

Received 16th August 2025,
Accepted 20th October 2025

DOI: 10.1039/d5bm01232e

rsc.li/biomaterials-science

Monocytes are mononuclear phagocytes crucial for tissue repair, pathogen clearance, and immune surveillance. Comprising 2–10% of all human blood peripheral leukocytes, monocytes are precursors to macrophages and dendritic cells and can be leveraged for diagnostics and treatment of various diseases, such as cancer and autoimmune conditions. Current methods of monocyte isolation for these applications, such as plastic adhesion, magnetic-activated antibody-based selection, and counterflow centrifugal elutriation are limited by either low purity and viability or costly equipment and reagents. Here, we develop and optimize an aptamer-based method for traceless isolation of monocytes from peripheral blood mononuclear cells at low cost with high purity and yield, and with minimal activation and immunogenic risks. We identify and use CD36 as a novel selection marker for monocyte isolation and confirm that monocytes isolated using our CD36-binding aptamer possess similar phenotypes to monocytes isolated from anti-CD14 and anti-CD36 antibodies with higher, unperturbed CD14 and CD36 expression.

Open Access Article. Published on 27 October 2025. Downloaded on 4/18/2026 8:16:51 AM.
This article is licensed under a Creative Commons Attribution-NonCommercial 3.0 Unported Licence.

## 1. Introduction

Monocytes are mononuclear phagocytic leukocytes that play a critical role in the innate immune system. As precursors to macrophages and dendritic cells, monocytes derive from the bone marrow, circulate in the blood, and migrate to inflammation sites to perform phagocytosis, antigen presentation, and cytokine production functions.[1–3] Due to their circulatory nature and distinct expression of pattern recognition receptors, monocytes are key players in tissue repair, bacterial and viral clearance, and immune surveillance. Understanding monocytes and leveraging their function can lead to therapeutics targeting various diseases, for example in monocyte cell therapy or in monocyte-based drug delivery.[4–6]

Monocytes and their derived cells, including dendritic cells and macrophages, have shown great potential as cell therapies in oncology due to their enhanced homing abilities and efficient drug delivery properties.[4] The first cell therapy approved by the U.S. Food and Drug Administration (FDA) was a dendritic cell vaccine for treatment of prostate cancer developed by Dendreon Pharmaceuticals in 2010.[7,8] More recently, Carisma Therapeutics received FDA clearance for an Investigational New Drug Application (IND) using a CAR-macrophage to target solid tumors overexpressing human epidermal growth factor receptor 2 (HER-2).[9] This CAR-macrophage therapy is reportedly more effective than CAR T cells in targeting solid tumors, due to more diverse antitumor mechanisms and better infiltration ability.[9,10] Additionally, there are currently over 120 dendritic cell and 11 macrophage cell therapies in clinical trials, targeting diseases from cancer to stroke.[7]

Monocytes comprise only about 2–10% of all human peripheral blood leukocytes.[11] Thus, high purity isolation of viable monocytes is a challenge for downstream applications. In addition, monocytes have limited proliferation capacity,[12] requiring high yields of isolation for therapeutic use. Isolation of monocytes from peripheral blood mononuclear cells (PBMCs) must (1) recover high purity monocytes with minimal contamination from lymphocytes, granulocytes, and platelets, and (2) preserve the desired phenotype and function for monocyte differentiation. Existing methods to isolate monocytes from blood products include plastic adhesion, counterflow centrifugal elutriation (CCE), magnetic bead-based depletion, and magnetic bead-based positive selection (Table 1).[7,13,14]

Plastic adhesion, although simple and cheap to perform, results in low monocyte yield (<13%) and purity (<50%) due to high contamination by platelets and lymphocytes.[7,13] This process also potentially induces monocyte activation, negatively affecting macrophage and dendritic cell differentiation.[15]

[a]*Molecular Engineering and Sciences Institute, University of Washington, Seattle, WA 98195, USA. E-mail: spun@uw.edu*
[b]*Department of Bioengineering, University of Washington, Seattle, WA 98195, USA*
[c]*Center for Fundamental Immunology, Benaroya Research Institute, Seattle, WA 98101, USA*

Open Access Article. Published on 27 October 2025. Downloaded on 4/18/2026 8:16:51 AM. This article is licensed under a Creative Commons Attribution-NonCommercial 3.0 Unported Licence.

Table 1 List of the advantages and disadvantages of current methods used to isolated monocytes from PBMCs

| Method | Description | Advantages | Disadvantages |
|---|---|---|---|
| Plastic adhesion | Plate cells on a plastic cell culture surface and detach adherent cells chemically or mechanically | Cheap; no specialized equipment needed; simple procedure | Low purity; low yield; high contamination of lymphocytes; risk of cell activation |
| Centrifugation-based methods | Use centrifugal forces in a chamber to separate cells based on size | Good purity; excellent yield | Requires expensive, specialized equipment; long/complex setup procedure |
| Magnetic negative selection with antibodies | Label contaminant cells with a cocktail of various antibody-conjugated magnetic beads and separate *via* magnet | Good purity; good yield; traceless/low risk of cell activation | Requires expensive antibody reagents and specialized magnetic equipment; high contamination of lymphocytes and platelets |
| Magnetic positive selection with antibodies | Label desired cells with antibody-conjugated magnetic beads and separate *via* magnet | Excellent purity; excellent yield | Requires expensive antibody reagents and specialized magnetic equipment; risk of cell activation; risk of immunogenicity |
| Magnetic positive selection with aptamers | Label desired cells with aptamer-conjugated magnetic beads and separate *via* magnet | Excellent purity; good yield; aptamers are >40-fold cheaper than antibodies; traceless/low risk of cell activation; low immunogenicity | Requires specialized magnetic equipment |

CCE uses centrifugal force and counterflow drag force to separate monocytes from PBMCs based on size and cell cycle stage. Although CCE recovers monocytes with high purity (>80%) and yield (>90%), it currently requires sole source supplies, expensive equipment, and large volumes of starting material.[16,17] Also, despite the fast separation speed of cell isolation (about 1 h for isolation of $20 \times 10^9$ cells), the setup, decontamination, and assembly of the complex equipment adds at least 4 h to sample processing.[7]

Magnetic bead-based depletion and positive selection use antibody-coupled magnetic beads and magnetic columns to rapidly enrich monocytes from PBMCs in 1–2 h. Depletion, or negative selection, employs an antibody cocktail to retain non-monocytes in the magnetic column and allow untouched monocytes to flow through the column. Unlabeled monocytes minimize the risk of activation. Isolation by depletion also results in reasonable yield (40–61%) and product purity (60–85%), but with contamination from platelets and granulocytes.[7,13,16,18,19] Positive selection utilizes anti-CD14 antibody-coupled magnetic reagents to retain $CD14^+$ monocytes on the magnetic column while washing out remaining cells, followed by monocyte recovery *via* removal of the magnetic field. This approach, which is the commonly preferred method of monocyte isolation, consistently results in the highest purity (>90%) and yield (>70%) compared to the aforementioned approaches.[7,13,16,17,19] However, eluted cells can still be bound to anti-CD14 magnetic beads, risking cell activation, immunogenicity, and phenotype changes.[7,20] Additionally, magnetic bead-based isolation is expensive, requiring antibodies and specialized magnetic equipment.

Aptamer-mediated cell selection is a promising alternative to antibody-conjugated magnetic bead-based positive selection.[21–25] Aptamers are single-stranded nucleic acid molecules that fold into structures that bind to protein, small-molecule, and cell targets with high specificity and affinity similar to antibodies.[26,27] Compared to antibodies, aptamers are less expensive and faster to synthesize with lower batch-to-batch variability, easier chemical modification, longer shelf life, and higher stability among a wider range of pH, ionic conditions, and temperature.[26,28–30] The major advantage of aptamer ligands over antibody ligands for cell isolation is the reversibility of binding, which can result in traceless target selection.[21–23] Here, we use a monocyte-binding aptamer and its complementary reversal strand to successfully isolate label-free monocytes from PBMCs with high purity and yield. Aptamer-based, label-free isolation of monocytes mitigates immunogenicity and activation concerns associated with antibody-based positive selection, thereby reducing potential phenotype alterations during monocyte differentiation. We first characterize the binding receptor for our previously discovered monocyte-binding aptamer as CD36. We then identify and use CD36 as a novel selection marker for monocyte isolation from PBMCs *via* a label-free, aptamer-mediated, cell selection platform. We lastly compare the phenotypes between monocytes and their derived macrophages isolated from anti-CD14 antibody (CD14 Ab), anti-CD36 antibody (CD36 Ab), and aptamer.

## 2. Materials and methods

### 2.1 Cell culture and PBMC isolation

THP-1 monocytes (Cat #TIB-202, ATCC) were cultured with RPMI 1640 medium (Corning) supplemented with 10% heat-inactivated fetal bovine serum (FBS, Life Tech). HEK293T cells (Cat #CRL-2316, ATCC) were cultured with DMEM medium (Gibco) supplemented with 10% heat-inactivated FBS. Human peripheral blood mononuclear cells (PBMCs) were isolated from Leukocyte Reduction System (LRS) cones (Bloodworks Northwest) *via* Ficoll-Paque (GE) density gradient centrifugation.[31] PBMCs were cryopreserved in RPMI containing 20% FBS and 10% DMSO (Sigma) before monocyte isolation procedures. Isolated monocytes were cultured in RPMI containing 10% FBS and 40 ng $mL^{-1}$ human macrophage colony-stimulating factor (M-CSF) (Cat #574804, BioLegend).

 This journal is © The Royal Society of Chemistry 2025

Open Access Article. Published on 27 October 2025. Downloaded on 4/18/2026 8:16:51 AM. This article is licensed under a Creative Commons Attribution-NonCommercial 3.0 Unported Licence.

### 2.2 Aptamer target receptor pull-down assay

Membrane protein extraction and aptamer pull-down method was performed as previously described.[32] For each group (control and CD36Apt), about $100 \times 10^6$ human monocytes were washed three times to remove media proteins and lysed in 3.3 mL of hypotonic buffer containing 10 mM Tris–HCl, pH 7.5 with Protease Inhibitor Cocktail (ThermoFisher Scientific) and 1 mM phenylmethylsulfonyl fluoride (PMSF, ThermoFisher Scientific) at 4 °C for 30 min under gentle rotation. Membrane debris was pelleted at 16 000*g* at 4 °C for 15 min and washed three times with 3.3 mL of hypotonic buffer to eliminate intracellular proteins. Membrane pellets were washed with 1 mL of Dulbecco's phosphate-buffered saline (DPBS, Corning) with $Mg^{2+}$ and $Ca^{2+}$, 5 mM $MgCl_2$, and 25 mM glucose (Wash Buffer, WB) supplemented with 1% Triton X-100, protease inhibitors, and 1 mM PMSF under gentle rotation and sonicated for 5 min in an ice water bath to extract membrane proteins. Samples were centrifuged and the supernatant containing the solubilized membrane proteins was stored at −80 °C before use.

Membrane extracts were first pre-cleared by incubation with 100 nM biotinylated nonspecific (NS) aptamer and 0.1 mg $mL^{-1}$ tRNA for 30 min at 4 °C. Then, 2 mg of MyOne Streptavidin C1 Dynabeads (ThermoFisher Scientific) pre-washed in WB 0.01% Triton X-100 were added to each membrane extract and incubated for 15 min at 4 °C. The solution was then placed on a magnetic rack to remove any nonspecific protein binders. The membrane extract supernatants were added to either a biotin control containing 1.5 mg of Streptavidin C1 Dynabeads pre-saturated with 50 nmol of biotin for 15 min at 4 °C or a CD36Apt aptamer fraction containing 100 nM biotinylated CD36Apt aptamer and 0.1 mg $mL^{-1}$ salmon sperm DNA. Extracts were incubated with Dynabeads for 30 min at 4 °C under gentle rotation. Target proteins were eluted by heating to 37 °C for 10 min in 50 μL of SDS loading buffer supplemented with beta-mercaptoethanol (BME), 10 mM EDTA, and 4.5 M urea. Eluted proteins were submitted for mass spectrometry analysis or denatured at 47 °C for 15 min and run on a 4–20% Tris–Glycine gel in the Novex XCell SureLock Mini-Cell Electrophoresis System (ThermoFisher Scientific). The gel was run at 190V for 15 min, then at 220V for 30–45 min. Gels were rinsed with water and stained with colloidal blue stain (Invitrogen) according to the manufacturer's instructions.

### 2.3 Flow cytometry binding assays

For antibody binding assays, cells ($0.2 \times 10^6$) were blocked using FcR blocking reagent, human (Miltenyi) according to the manufacturer's protocol. The following dyes and antibodies were used to stain cells: Zombie Violet (1 : 500 in 100 μL per $10^6$ cells, Cat #423114, BioLegend), FITC anti-human CD14 (1 : 50, Cat #301804, BioLegend), APC anti-human CD14 (1 : 20, Cat #301808, BioLegend), PE anti-human CD16 (1 : 40, Cat #12-0168-4, eBioscience), FITC anti-human CD36 (1 : 20, Cat #336203, BioLegend), PE anti-human CD36 (1 : 100, Cat #336205, BioLegend), BV711 anti-human CD163 (1 : 20, Cat #333629, BioLegend), PE-Cy7 anti-human HLA-DR (1 : 200, Cat #327017, BioLegend), FITC anti-human CD80 (1 : 20, Cat #305206, BioLegend), APC anti-human CD86 (1 : 20, Cat #305411, BioLegend), APC anti-human CD206 (1 : 100, Cat #321110, BioLegend) and AF647 streptavidin (1 : 500, Cat #405237, BioLegend). Unstained and single-stained samples were prepared for compensation controls. Fixed cells were analyzed on an Attune NxT (Invitrogen) flow cytometer.

For aptamer binding assays, biotinylated and Cy5-labeled aptamers (nonspecific aptamer sequence, CD36Apt, CD36Apt.65) were annealed at 95 °C for 5 min and snap-cooled on wet ice for at least 10 min. Aptamer sequences were ordered from Integrated DNA Technologies and can be found in Table S1. Cells were incubated with folded aptamers in WB further supplemented with 0.1 mg $mL^{-1}$ salmon sperm DNA and 0.1 mg $mL^{-1}$ tRNA (Binding Buffer, BB) at 4 °C for 20 min. After binding, cells were washed twice with 200 μL of WB with 1% bovine serum albumin (BSA, Miltenyi) and incubated with secondary AF647 streptavidin stain at 4 °C for 20 min, if necessary. After secondary staining, cells were washed twice with 200 μL of WB 1% BSA and fixed with 200 μL of WB 1% BSA 0.1% paraformaldehyde (PFA, ThermoFisher Scientific).

For aptamer and antibody co-staining assays, cells blocked with FcR blocking reagent were incubated with both a Cy5-labeled CD36Apt.65 aptamer (100 nM) and the appropriate antibody listed above at 4 °C for 20 min. Cells were washed and fixed as described above.

### 2.4 Bio-layer interferometry

Bio-layer interferometry (BLI) was completed on a ForteBio Octet Red96 instrument. Streptavidin biosensors (Sartorius) were loaded with 50 nM biotinylated CD36Apt.65 aptamer until a capture threshold of 0.5 nm was reached. After 120 s rinse and baseline steps in buffer only, sensors were added to a dilution series of recombinant human CD36-His protein (Acro Biosystems) ranging from 6.25 to 100 nM in concentration. Association with protein was monitored for 118 s and dissociation with buffer only was carried out for 134 s. Data was analyzed using the Octet Data Analysis 9.0 (ForteBio) and binding parameters were calculated with a global fit on all kinetic curves generated from the dilution series of protein binding.

### 2.5 Binding of CD36Apt to plasmid-transfected HEK293T cells

mCherry-CD36-C-10 was a gift from Michael Davidson (Addgene plasmid #55011). $50 \times 10^3$ $CD36^-$ HEK293T cells were grown for 24 h in tissue culture-treated 24-well plates and then transfected with 0.5 μg of the plasmid and 1.5 μL of Lipofectamine 3000 Reagent (ThermoFisher Scientific), according to the manufacturer's instructions. Cells were examined 24 h after transfection for mCherry expression, FITC anti-CD36 antibody binding, and Cy5-labeled CD36Apt binding *via* flow cytometry.

### 2.6 Reversal agent optimization

Reversal agents of 18, 23, and 27 nucleotides (nt) were designed complementary to the 3′ end of CD36Apt.65. THP1

Open Access Article. Published on 27 October 2025. Downloaded on 4/18/2026 8:16:51 AM. This article is licensed under a Creative Commons Attribution-NonCommercial 3.0 Unported Licence.

cells bound first with 25 nM CD36Apt.65 aptamer and secondary AF647 streptavidin labelling, as described above, were incubated with 10-, 50-, and 100-fold excesses (over aptamer amount) of 100 μL of reversal agent in WB 1% BSA at room temperature for 10 min. Cells were washed twice with WB 1% BSA to remove unbound aptamers, fixed, and analyzed with flow cytometry.

### 2.7 CD36Apt.65-mediated magnetic isolation

Thawed PBMCs or a mix of cultured THP1 and Jurkat cells were incubated with various concentrations (6.25, 12.5, and 25 nM) of biotinylated CD36Apt.65 at 4 °C for 15 min under gentle rotation. Aptamer-labeled cells were washed twice with 10 mL of WB 1% BSA. Anti-biotin MicroBeads (Miltenyi Biotec) with different volumes (50, 100, 150, and 200 μL) were diluted to 500 μL and then incubated with aptamer-labeled PBMCs at 4 °C for 15 min under gentle rotation. Cells were washed twice with 10 mL of WB 1% BSA, resuspended in DPBS 0.5% BSA, and applied over one LS column (Miltenyi Biotec) on a QuadroMACS separator (Miltenyi Biotec) according to the manufacturer's protocols. The flowthrough fraction was collected, consisting of initial unbound cells that passed through column and three 3 mL column washes of DPBS 0.5% BSA 1 mM EDTA. Next, 1 mL of 100-fold excess 23 bp reversal agent was added to the column in DPBS 0.5% BSA. About 600 μL (column void volume) of the solution was passed before the column was plugged for 10 min at room temperature. Afterward, the column was washed with three 3 mL column washes of DPBS 0.5% BSA 5 mM EDTA in the reversal agent elution (RAE) fraction. Cells remaining on the column were flushed out with 5 mL DPBS 0.5% BSA 1 mM EDTA using a plunger. All fractions (flowthrough, RAE, flush) were counted and analyzed *via* flow cytometry with Cy5-CD36Apt.65 (100 nM) and FITC anti-human CD14 or APC anti-human CD14, PE anti-human CD16, FITC anti-human CD36, PE-Cy7 anti-human HLA-DR, and BV711 anti-human CD163. Monocyte isolation with CD14 MicroBeads (Cat #130-050-201, Miltenyi Biotec) and biotinylated CD36 Ab (Cat #130-099-744, Miltenyi Biotec) were carried out according to manufacturer's instructions.

### 2.8 Macrophage differentiation and polarization

For differentiation of monocytes into macrophages (monocyte-derived macrophages, MDMs), $1 \times 10^6$ isolated cells were cultured in non-treated 6-well plates in RPMI 1640 with 10% FBS and 40 ng $mL^{-1}$ M-CSF for 7 days, with media change every 3–4 days. After MDM differentiation, cells were washed twice with DPBS and stimulated with 50 ng $mL^{-1}$ LPS and 10 ng $mL^{-1}$ IFN-γ for M1 polarization, 20 ng $mL^{-1}$ IL-4 for M2 polarization, or left untreated as M0 macrophages. MDMs were detached with an incubation in 2 mM EDTA in DPBS over ice for at least 20 min and gentle scraping/pipetting.

### 2.9 RNA extraction and quantitative PCR

RNA from polarized macrophages were extracted with a RNeasy Mini Kit (Cat #74104, Qiagen) according to the manufacturer's instructions. Briefly, cells were lysed with RLT buffer supplemented with BME and mixed in a 1 : 1 ratio with 70% ethanol. Samples were then transferred to RNeasy spin columns, centrifuged, and washed with RW1 and RPE buffer. Purified RNA was eluted in nuclease-free $H_2O$ and measured by a NanoDrop One Spectrophotometer (ThermoFisher Scientific).

RNA was reverse transcribed to cDNA using the High-Capacity cDNA Reverse Transcription Kit with Rnase Inhibitor (Cat #4374967, Applied Biosystems), according to the manufacturer's protocol. RNA was transcribed in 20 μL reactions. Quantitative polymerase chain reaction (qPCR) was performed using the 7300 Real-Time PCR System (Applied Biosystems). cDNA was diluted 1 : 10 in 25 μL total reactions with PowerUp SYBR Green Master Mix (Applied Biosystems). Primer sequences are listed in Table S2. qPCR reactions were incubated at 50 °C for 2 min, 95 °C for 2 min, followed by 40 cycles of 95 °C for 15 s, 56 °C (primer-specific annealing temperature) for 15 s, and 72 °C for 1 min.

### 2.10 Soluble cytokine measurements

After macrophage polarization, 500 μL of cell culture supernatants were collected and frozen at −20 °C until ready to analyze *via* LEGENDplex (BioLegend) for IL-6 and TNFα, using Detection Antibodies (Cat #741041), Standard (Cat #741042), IL-6 Capture Beads (Cat #740044), and TNFα Capture Beads (Cat #740053). Thawed supernatants, diluted 1 : 2 or 1 : 10 in Assay Buffer, were captured on beads and detected with biotinylated antibodies tagged with streptavidin-PE fluorophore, according to the manufacturer's protocol. Captured cytokines were analyzed by flow cytometry.

### 2.11 Phagocytosis assay

$0.1 \times 10^6$ monocytes were plated in 96-well plates and allowed to adhere for 1 h. 1 or $5 \times 10^6$ *Escherichia coli* bioparticles, Alexa Fluor™ 488 conjugate (Thermo Fisher) were added to the cells and spun down for 1 min at 300*g*. Monocytes were incubated with the bioparticles at 37 °C for 30 min, washed with DPBS over ice, and then analyzed on the flow cytometer.

### 2.12 TLR agonist assay

$0.5 \times 10^5$ monocytes were plated in 96-well plates and allowed to adhere in serum-free RPMI for 1 h. Media was replaced with complete RPMI and cells were allowed to recover for 2 h. TLR agonists PAM3CSK4 (Invivogen) and S. Enterica 595 LPS (List Biological Labs) were added at 1 μg $mL^{-1}$ and 10 ng $mL^{-1}$, respectively, and cells were incubated at 37 °C overnight. Cell culture supernatants were collected and analyzed for IL-6 and TNF-α concentrations *via* the bead-based LEGENDplex (BioLegend) assay, as previously mentioned.

## 3. Results and discussion

### 3.1 Characterization of CD36Apt binding and receptor identification

We previously identified a monocyte-binding aptamer (Mono. A2) that binds to human monocytes with a dissociation con-

 This journal is © The Royal Society of Chemistry 2025

Open Access Article. Published on 27 October 2025. Downloaded on 4/18/2026 8:16:51 AM. This article is licensed under a Creative Commons Attribution-NonCommercial 3.0 Unported Licence.

stant ($K_D$) of 45 (±9.1) nM using cell-SELEX (systematic enrichment of ligands using exponential enrichment).[33] Despite the high specificity of Mono.A2 binding to CD14$^+$ cells in PBMCs, the aptamer does not bind to recombinant CD14 or CD14-transfected Jurkat cells.[33] Because receptor identification by pulldown assay requires large numbers of human monocytes, we used Mono.A2 to isolate monocytes from PBMCs using the aptamer-mediated cell selection method detailed in the next section. We then applied a reported aptamer pull-down assay to identify the target membrane receptors of the aptamer.[32,34,35] In brief, we bound biotin-Mono.A2 to monocyte cell membrane extracts, extracted aptamer-bound membrane proteins with Streptavidin Dynabeads, and analyzed the recovered proteins *via* SDS-PAGE and mass spectrometry. Compared to a control sample isolated with biotin-saturated streptavidin beads lacking Mono.A2, we observed one protein band enriched by Mono.A2 at approximately 200 kDa (Fig. S1). Using mass spectrometry analysis on the aptamer-recovered proteins compared to the control proteins, we cross-referenced identified membrane proteins with relevant monocyte surface markers *via* the UniProt database and identified CD36 as the potential binding receptor of the Mono.A2 aptamer, which we renamed to CD36Apt.

We next validated that CD36Apt indeed binds human CD36 by three methods: (i) co-staining of aptamer with CD36 Ab, (ii) BLI with aptamer and recombinant human CD36 protein, and (iii) CD36 knock-in expression in CD36$^-$ cells. To first confirm CD36Apt binding to CD36, we co-stained human monocytes with CD36Apt and anti-CD36 antibody. We observed a positive, linear correlation between the aptamer and Ab stains, indicating that CD36Apt can bind to CD36 on monocytes at the same time as CD36 Ab (Fig. 1A). Next, we transiently transfected CD36$^-$ HEK293T cells with CD36 from mCherry reporter plasmid mCherry-CD36-C-10. We first confirmed that CD36Apt does not bind to parental, non-transfected HEK293T cells (Fig. S2). Transient CD36 expression resulted in CD36Apt aptamer binding specific to mCherry$^+$ cells (Fig. 1B). Finally, we applied BLI to characterize the binding kinetics of CD36Apt to recombinant human CD36 protein. We immobilized biotin-CD36Apt onto streptavidin biosensors and monitored binding to serially diluted human CD36-His protein. CD36Apt bound the CD36 protein with a $K_D$ of 26.3 nM (Fig. 1C).

CD36 is a Class B scavenger receptor consisting of 472 amino acids with an apparent molecular weight of 88 kDa.[36,37] CD36 forms homodimers and multimers *via* thiol bridging between extracellular cysteine residues, which provides a possible explanation for the distinct higher molecular weight band of CD36 in the aptamer pull-down assay gel.[38,39] Within PBMCs, CD36 is uniquely expressed on CD14-expressing monocytes; however, it is also expressed on various other cells,

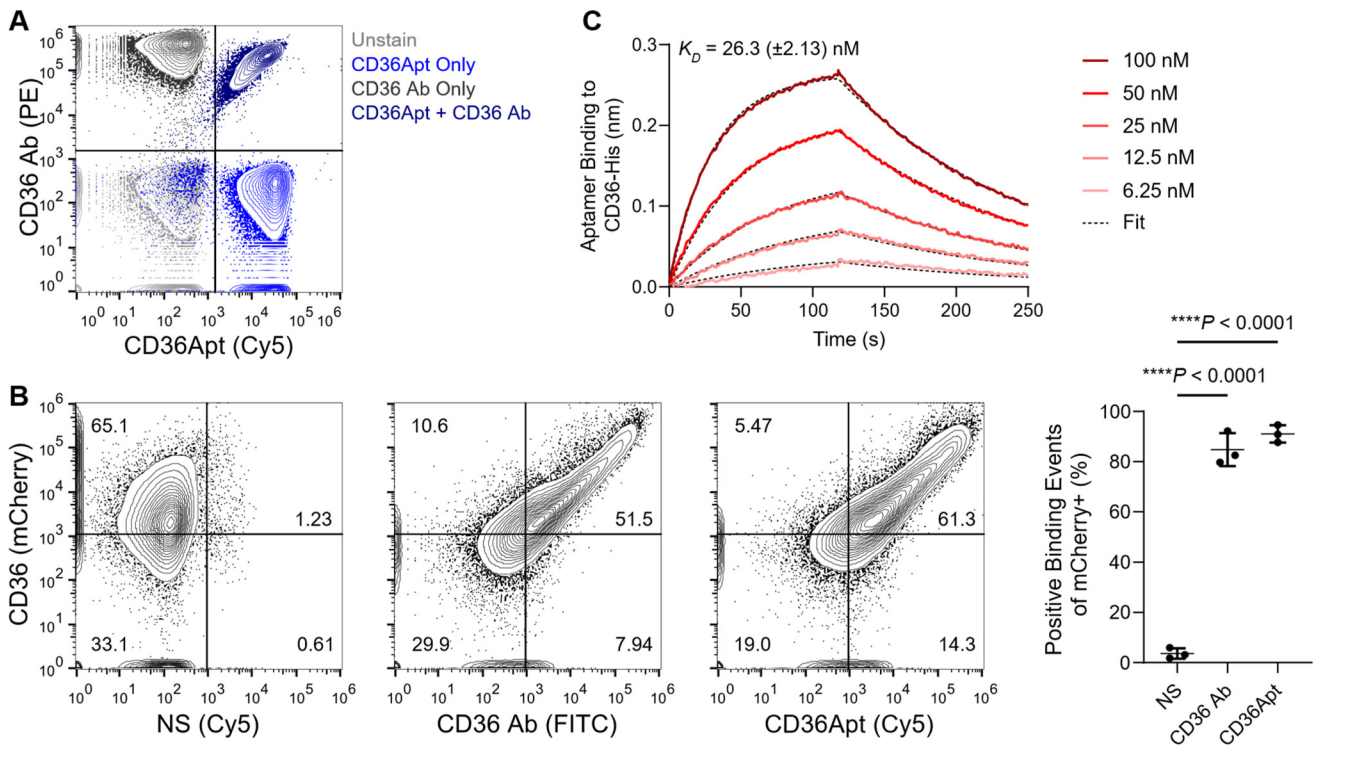


**Fig. 1** CD36Apt binds to CD36 receptor on monocytes. (A) Flow cytometry plots of monocytes co-stained with anti-CD36 antibody (CD36 Ab) and monocyte-binding aptamer (CD36Apt). (B) Representative flow cytometry plots of nonspecific aptamer (NS), CD36 Ab, and CD36Apt binding to CD36$^-$ HEK293T cells 24 h after lipofectamine transfection with mCherry-CD36-C-10 plasmid (left) and graph of percentage of mCherry$^+$ HEK293T cells that were also positive for antibody and aptamer binding (right). Horizontal lines and error bars represent the mean and s.d. of technical triplicate experiments; $n$ = 3; ****$P$ < 0.0001 (one-way ANOVA). (C) Association and dissociation kinetic curves from BLI of various concentrations of CD36-His protein binding to immobilized biotin-CD36Apt.

Open Access Article. Published on 27 October 2025. Downloaded on 4/18/2026 8:16:51 AM. This article is licensed under a Creative Commons Attribution-NonCommercial 3.0 Unported Licence.

including macrophages, adipocytes, microglia, microvascular endothelial cells, and platelets.[40–43] CD36 contains one large extracellular domain, two transmembrane domains, and two short cytosolic regions.[37,44] CD36 binds to numerous ligands, such as thrombospondin, long-chain fatty acids, and pathogen-associated molecular patterns, corresponding to diverse functions in angiogenesis, fatty acid transport and metabolism, and the immune response, respectively.[45–49] To our knowledge, only one other CD36-binding aptamer is reported in the literature, discovered from cell-SELEX with nonalcoholic fatty liver disease cells.[50] However, this aptamer demonstrated no binding to monocytes or to human recombinant CD36 protein *via* flow cytometry and BLI, respectively, in our experimental conditions (Fig. S3). Because CD36 undergoes alternative splicing, one potential explanation is that the aptamers may bind different CD36 isoforms on different cell types.[51]

### 3.2 Optimization of traceless, aptamer-based isolation of monocytes

Currently, anti-CD14 antibody is used in positive magnetic selection to isolate highly pure monocytes for downstream applications. However, the magnetic beads can remain bound to CD14 on monocytes for days in culture, resulting in impaired activation and proliferation of monocytes in response to stimuli.[52] We hypothesize that CD36 can be alternatively used to isolate pure, viable monocytes from PBMCs. Like CD14, CD36 also differentiates between classical and nonclassical monocyte subsets.[53,54] In addition, unlike some other monocyte markers, such as CD163, CD36 expression is not affected by anticoagulants or cell processing methods.[55] Therefore, we evaluate here the feasibility of using CD36Apt for monocyte isolation and characterize the isolated cell products compared to anti-CD14 antibody and anti-CD36 antibody.

We first truncated CD36Apt from 88 nucleotides (nt) to 65 nt in the stem region, preserving the NUPACK-predicted binding loops and creating an 8 nt toehold sequence for fast strand displacement with the reversal agent (Fig. S4A). We renamed the 65 nt, truncated CD36Apt "CD36Apt.65". We confirmed binding of CD36Apt.65 to CD36 on THP1 cells (Fig. S4B) and then designed reversal agents of 18, 23, and 27 nt in length to maximize release of CD36Apt.65-bound cells (Fig. S4C). To determine the optimal reversal agent length, we evaluated the ability of the reversal agent to reverse binding of fluorescently-labeled CD36Apt to THP1 cells. We tested reversal agent concentrations (10- to 100-fold excess of aptamer) at room temperature for 10 min. With >92% aptamer release at 100-fold excess, the 23 nt reversal agent displaced CD36Apt.65 most effectively from THP1 cells at all concentrations (Fig. S4D). Thus, we selected the 23 nt reversal agent for further use in our traceless, aptamer-mediated monocyte isolation platform.

For label-free, aptamer-mediated isolation of monocytes from PBMCs, we incubated PBMCs with CD36Apt.65 aptamer immobilized on magnetic Anti-Biotin Microbeads (Miltenyi Biotec), ran those cells through a magnetic column that captured aptamer-labeled cells and eliminated undesired subsets in the flowthrough fraction *via* washing, and eluted the captured cells with a 10 min incubation using the complementary reversal agent in the reversal agent elution fraction (RAE), which disrupted the secondary structure imperative for cell binding (Fig. 2A). Any remaining cells were flushed off the column in the flush fraction. All fractions were analyzed with flow cytometry staining (Fig. S5).

We optimized the aptamer-mediated cell selection platform by (1) titrating aptamer concentrations, (2) varying ratios of magnetic beads to cell number, (3) changing formulations of column wash buffer, and (4) testing different conditions of reversal agent incubations. We first evaluated various aptamer loading conditions on magnetic supports for optimal purity and cell capture. We incubated the magnetic beads with CD36Apt.65 aptamer at 6.25, 12.5 and 25 nM, removed unbound aptamers by washing, and then incubated the aptamer-coupled beads with PBMCs. We found that the magnetic bead pre-incubation with 25 nM of aptamer captured 90% of $CD14^+$ monocytes compared to the 51% and 12% cell capture using magnetic beads incubated with 12.5 and 6.25 nM of aptamer, respectively. Comella *et al.* also previously showed that an increase in antibody concentration led to an increase in cell magnetophoretic mobility on separation of natural killer cells from PBMCs using MACS. This increased cell mobility provided higher cell capture with 40 μL compared to 1 μL of antibody.[56] However, purity values were higher for the lower concentrations of aptamer (Fig. S6A). We have previously seen a decrease in purity with higher immobilized aptamer concentration in a resin-based cell selection system. Higher aptamer densities could disrupt aptamer folding and limit steric accessibility of immobilized aptamers for the cells.[57,58] We selected 25 nM of aptamer for the final protocol due to the success of cell capture with a small expense of purity. Next, we tested magnetic bead volumes of 50, 100, 150, and 200 μL per 100 million PBMCs. Although higher bead volumes were shown to improve magnetic bead labelling and cell capture,[59,60] we observed no difference in purity or yield with different bead volumes, possibly due to the excess of magnetic beads compared to aptamer-bound cells (Fig. S6B). We selected 50 μL beads per 100 million PBMCs for the final protocol to maximize purity and yield and minimize cost. We then tested variations of column wash buffers with 0.5–1% BSA and 1–2 mM EDTA formulated in DPBS solution. There were no significant changes in purity or yield between these column wash buffer formulations (Fig. S6C), so we selected the 0.5% BSA and 1 mM EDTA formulation as the column wash buffer to minimize cost.

Finally, we evaluated several methods to increase cell elution efficiency, including (1) increasing reversal agent incubation time, (2) adding a second reversal agent incubation, and (3) increasing the reversal agent incubation temperature. Increasing DNA hybridization time has been shown to improve binding of DNA complementary strands.[61,62] We thus increased the incubation time for reversal agent-aptamer binding from 10 min to 20 min but observed only minimal

 This journal is © The Royal Society of Chemistry 2025

Open Access Article. Published on 27 October 2025. Downloaded on 4/18/2026 8:16:51 AM.
This article is licensed under a Creative Commons Attribution-NonCommercial 3.0 Unported Licence.

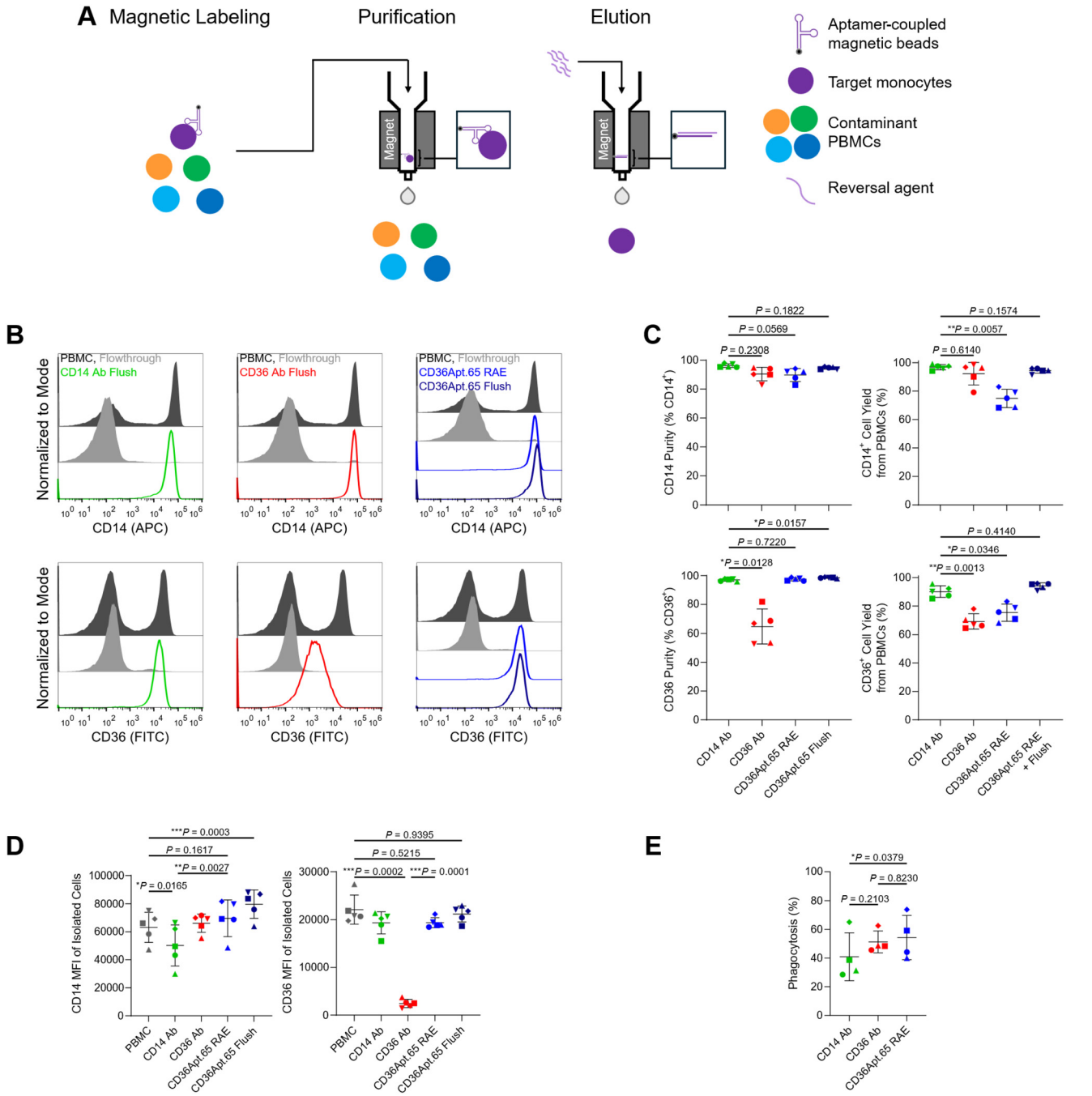


**Fig. 2** Traceless isolation of monocytes from PBMCs using aptamer-mediated selection. (A) Scheme demonstrating aptamer-mediated cell selection, where PBMCs incubated with biotin-aptamer coupled onto anti-biotin magnetic beads that specifically labeled monocytes were applied to an LS column on a magnet, which removed unlabeled cell in the flowthrough. Aptamer-labeled cells were then incubated with 100-fold excess of the reversal agent and eluted from the column in the reversal agent elution (RAE) fraction. Remaining cells were flushed out with a column plunger. (B) Representative flow cytometry plots of CD14 (top) and CD36 (bottom) expression in different cell fractions of CD14 Ab-based (left), CD36 Ab-based (middle), and CD36Apt.65-based (right) isolations. (C) Flow cytometry analysis of purity and yield of different fractions of Ab and aptamer-based isolations, based on $CD14^+$ (top) and $CD36^+$ (bottom) cell populations. (D) Flow cytometry analysis of CD14 (left) and CD36 (right) MFI of isolated cells. (E) Flow cytometry analysis of number of phagocytic monocytes based on percent uptake of *E. coli* particles. Circles, squares, triangles, and diamonds correspond to different donors. Horizontal lines and error bars represent the mean and s.d.; $n = 5$ (C and D), $n = 4$ (E); $P > 0.5$, $^*P < 0.05$, $^{**}P < 0.01$, $^{***}P < 0.001$, $^{****}P < 0.0001$ (paired one-way ANOVA).

improvements in purity and no improvement in yield (Fig. S6D, left). We also implemented a second reversal agent incubation to improve the efficiency of reversal agent elution, but again did not see any notable differences in purity or yield (Fig. S6D, middle). Next, we hypothesized that increasing the temperature of reversal agent incubation would increase the

Open Access Article. Published on 27 October 2025. Downloaded on 4/18/2026 8:16:51 AM. This article is licensed under a Creative Commons Attribution-NonCommercial 3.0 Unported Licence.

hybridization efficiency and/or disrupt binding of the aptamer to the cells, thereby releasing more bound cells. Rashid *et al.* showed that a slight increase in temperature improved hybridization efficiency due to a higher kinetic rate of hybridization.[62] However, we observed a decrease in cell purity and a slight decrease in cell yield at the higher incubation temperature (Fig. S6D, right). Increasing the temperature (at temperatures much lower than the melting temperature) would also decrease the free energy of hybridization,[63] potentially decreasing aptamer-reversal agent interactions. It is possible that the higher temperature caused aptamer-reversal agent reactions to be unstable, while the aptamer-target cell interactions were not affected. However, we did not test CD36Apt.65 binding to monocytes at temperatures higher than 4 °C due to aptamer internalization concerns.[33] Our final isolation conditions were 25 nM of CD36Apt.65 aptamer, 50 μL of Anti-Biotin Microbeads per 100 million PBMCs, 0.5% BSA and 1 mM EDTA in the column wash buffer, and one 100-fold excess reversal agent incubation of 10 min at room temperature.

### 3.3 Comparison of peripheral blood monocytes by CD14 antibody, CD36 antibody, and CD36 aptamer selection

We compared monocyte isolation from five separate PBMC donors using our optimized CD36Apt.65 approach, antibody-based CD14 Microbeads (Miltenyi Biotec), and CD36 Ab immobilized on Anti-Biotin Microbeads. We confirmed efficient depletion of $CD14^+$ cells from the flowthrough fractions of all isolation strategies corresponding to high enrichment of $CD14^+$ cells in either the RAE fraction for the aptamer or flush fractions for the antibodies, confirming that capture of monocytes from PBMC is comparable between CD36Apt.65 aptamer and antibody-based isolation.

Overall, the combined aptamer RAE and flush fractions yielded 94.4 (±1.80) % of the $CD14^+$ monocytes from the initial PBMC population, of which the RAE fraction alone yielded 74.8 (±6.44) %. These numbers are comparable to those obtained from CD14 Ab and CD36 Ab isolations, which yielded 96.9 (±1.90) % and 92.2 (±7.95) %, respectively (Fig. 2C, top right). On average, the purity of $CD14^+$ cells in the aptamer RAE fraction was 89.8 (±4.49) %, indicating low non-specific binding to other $CD14^-$ cells in the PBMC population and low capture levels of $CD36^+$ $CD14^-$ cells. Compared to the purity of $CD14^+$ cells in the CD14 Ab and CD36 Ab elution fractions, with 96.3 (±1.28) % and 90.4 (±4.69) %, respectively, the aptamer RAE purity is similarly very high (Fig. 2C, top left). The CD14 staining MFI values of the aptamer-isolated RAE fraction and the CD36 Ab elution fraction were also similar to that of the monocytes in the initial PBMC population with an insignificant variation of 4.6 and 10.1%, respectively. However, the CD14 MFI value of the CD14 Ab-isolated monocytes was substantially lower than the initial PBMC population, with a decrease of about 20.4% (Fig. 2D, left), likely due to the CD14 microbeads blocking binding of the CD14 antibody used for staining. The compromised anti-CD14 antibody binding after positive antibody-based selection highlights the advantage of traceless isolation, which leaves the receptor untouched, minimizing any activation or phenotypic skew for downstream applications. Because bound CD14 Ab reduces monocyte responsiveness to LPS stimulation, with decreased cytokine production and increased phagocytic capacity,[52,64,65] these results also support the use of CD36 as an alternative marker for monocyte isolation, which leaves CD14 unperturbed. In addition, proliferation of positively sorted $CD14^+$ monocytes can be impaired compared to negatively selected monocytes.[52] $CD14^+$ cells in the aptamer-isolated flush fraction were also very pure (94.6 ± 0.85%) and exhibited slightly higher CD14 and CD36 MFI values compared to the antibody flush fractions. The higher CD14 and CD36 MFI values on cells that remained in the column is consistent with the high expression of both markers on classical monocytes.[53] The higher CD36 expression likely made aptamer displacement more difficult *via* reversal agent elution.

The combined aptamer RAE and flush fractions yielded 94.2 (±2.16) % of the $CD36^+$ cells from the initial PBMC populations, with the RAE fraction alone yielding 75.4 (±5.97) %. Once again, yields from aptamer-based selection are comparable to the yields obtained from CD14 Ab and CD36 Ab selection of 90.1 (±4.09) % and 69.24 (±5.30) %, respectively (Fig. 2C, bottom right). The purity of $CD36^+$ cells in the aptamer RAE fraction was 97.5 (±1.09) % which was very similar to the purity of the CD14 Ab elution fraction, which was 97.0 (±0.89) %. Interestingly, these $CD36^+$ purity values were much higher than the $CD36^+$ purity from CD36 Ab isolation, which was only 64.8 (±12.1) % (Fig. 2C, bottom left). Given the high depletion of $CD36^+$ cells in the flowthrough of CD36 Ab-based isolation and the low purity of $CD36^+$ cells in the elution fraction, we hypothesize that the CD36 Ab might not have been specific to or had a lower affinity for $CD36^+$ cells in the PBMC population. Alternatively, although the CD36 Ab used to isolate cells (clone AC106) was different from that used for staining (clone 5–271), these separate clones could have competed against each other for binding, thereby reducing the apparent $CD36^+$ population and the CD36 MFI values compared to the CD14 Ab-based and aptamer-based isolations (Fig. 2D, right).

We also analyzed the isolated monocytes from all three strategies for CD163 expression, HLA-DR expression, and for monocyte subset populations. While reduced expression of M2 marker CD163 has been observed for monocytes isolated from positive and negative selection compared to initial PBMCs,[13] we did not see any change in CD163 expression in the elution fractions from the three different isolation methods (Fig. S7A). We did observe a decrease of CD163 expression in the CD36Apt.65 flush fraction, potentially due to some TLR activation during processing, leading to ectodomain shedding of CD163.[13,66] However, we observed no difference in CD163 expression levels between the aptamer RAE elution fraction and native PBMCs. We also observed no significant difference in HLA-DR expression between any of the isolation strategies (Fig. S7B). We analyzed the isolated monocytes for the three different monocyte subsets. Monocytes are categorized into three subsets: classical ($CD14^{++}$, $CD16^-$), intermediate

 This journal is © The Royal Society of Chemistry 2025

Open Access Article. Published on 27 October 2025. Downloaded on 4/18/2026 8:16:51 AM. This article is licensed under a Creative Commons Attribution-NonCommercial 3.0 Unported Licence.

(CD14$^+$, CD16$^+$), and non-classical (CD14$^+$, CD16$^{++}$). About 80–95% of circulating monocytes are classical monocytes, which exhibit high phagocytic capacity and rapidly migrate to infection sites.[67,68] The remaining 5–20% of circulating monocytes are intermediate or non-classical monocytes, which play a role in antigen presentation, T cell stimulation, and inflammatory responses.[67,68] Likewise, isolation methods did not impact the distribution of monocyte subsets, as the classical, intermediate, and non-classical populations of all isolated monocytes were similar to the initial PBMC distribution (Fig. S7C). Although we expected a decrease in non-classical populations of isolated monocytes compared to native monocytes, non-classical monocytes still express low levels of CD14 and CD36,[67] which could bind weakly to the affinity reagents.

We next evaluated the function of monocytes isolated from all three strategies *via* phagocytosis potential and response to toll-like receptor (TLR) agonists. CD14 is a critical pattern recognition receptor for lipopolysaccharide (LPS), a component of Gram-negative bacterial cell walls. The interaction of CD14 with multiple TLRs, such as TLR2, 4, and 6, greatly contributes to clearance of bacterial infections.[65] CD36 is a scavenger receptor but also functions as a pattern recognition receptor that mediates phagocytosis of bacterial pathogens.[48] Given the similar purities of CD14 and CD36 in isolated monocytes using CD14 Ab and CD36Apt.65, it is possible that the presence of magnetic beads attached to the surface of CD14 Ab-isolated monocytes could block LPS binding to CD14, interfering with phagocytosis of LPS-containing Gram-negative bacteria. The aptamer-isolated monocytes lack any bulky beads or receptor blocking, enabling proper binding of CD14 to LPS for bacterial clearance. To examine the phagocytic potential of the isolated monocytes, we incubated adhered monocytes with Alexa Fluor 488-labeled, heat-killed *E. coli* for 30 min, washed to remove free bacteria, then analyzed the cells by flow cytometry. We discovered a higher percentage of *E. coli* phagocytosis in the aptamer-isolated monocytes at 54.3 (±15.4) % compared to the CD14 Ab-isolated monocytes at 40.9 (±16.7) % (Fig. 2E). CD36 Ab-isolated monocytes also show higher phagocytosis than CD14 Ab-isolated monocytes, although not statistically significant, further supporting the receptor blocking hypothesis.

To analyze the inflammatory responses of the isolated monocytes, we treated them with agonists for the pattern recognition receptors TLR2 and TLR4. TLR2 binds to a variety of pathogenic di- or triacylated lipopeptides found in bacterial cell walls, forms heterodimers with other TLRs, such as TLR1, TLR6, and TLR10, and triggers the MyD88-dependent NF-κB signaling pathway for cytokine production.[69–72] TLR2 also interacts with co-receptors CD14 and CD36 for modulation of inflammatory responses.[73,74] TLR4 primarily binds to Gram-negative bacterial LPS *via* the MD-2 accessory protein, also activating MyD88 and NF-κB for the production of pro-inflammatory cytokines.[75,76] CD14 plays a large role in transporting LPS to the TLR4/MD-2 complex, facilitating TLR4 activation and its subsequent signaling.[77–79] CD36 has been shown to participate in bacterial clearance *via* cooperation with TLR4, but not *via* a direct interaction or complex with TLR4.[48,80,81] Therefore, we examined the pro-inflammatory cytokine responses of isolated monocytes to the TLR2 agonist PAM3CSK4 and the TLR4 agonist LPS and measured secretion of pro-inflammatory cytokines TNFα and IL-6. Collectively, there were no significant differences in cytokine production for IL-6 or TNFα in response to these TLR agonists between monocytes of different isolation methods (Fig. S8).

The CD36Apt.65 aptamer-mediated cell selection of monocytes from PBMCs was highly robust among three different donors, with high yield and purity isolations for both CD14$^+$ and CD36$^+$ cells. This approach eluted label-free monocytes with similar functional capacities to monocytes isolated with the standard anti-CD14 antibody bead-based approach, but with minimal concerns for activation or immunogenic effects in downstream manufacturing processes. This completely synthetic system also circumvents the need for complex and costly antibody production and shows potential for serial selection of multiple, different cell types in a single isolation apparatus.[21]

### 3.4 Phenotypic comparison of monocyte-derived macrophages from monocytes isolated *via* CD14 antibody, CD36 antibody, and CD36Apt.65

To evaluate the potential of using CD36Apt.65 as a selection agent in the production of macrophage cell therapies, we further characterized macrophages differentiated from monocytes isolated by CD14 Ab, CD36 Ab, and CD36Apt.65. Monocytes differentiate into macrophage subtypes depending on varying stimuli in different tissues. M1 macrophages exhibit a pro-inflammatory phenotype, contributing largely to antimicrobial and anti-tumor response *via* immune cell activation, ROS generation, and phagocytosis.[82,83] Thus, reprogramming macrophages to the M1 phenotype is an attractive therapy for cancer suppression.[84–86] M2 macrophages display an anti-inflammatory phenotype, integral to tissue repair, angiogenesis, and tumor metastasis.[84,87] It is important to note that macrophage polarization is characterized by high plasticity; macrophage subsets can adapt to changes in the environment.[88,89]

Here, we differentiated monocytes isolated by different methods for 7 days in M-CSF and polarized the macrophages to M0 (M-CSF), M1 (IFN-γ and LPS), and M2 (IL-4) for 48 h. We then analyzed these macrophages for (1) surface marker expression of M1 markers CD80 and CD86 and M2 markers CD36 and CD206 *via* flow cytometry staining, (2) gene expression levels of IL-6, TNFα, and CD206 *via* qPCR analysis, and (3) soluble cytokine measurements of IL-6 and TNFα cytokines.

We first analyzed the capacity of monocyte-derived macrophages (MDMs) to polarize to M0, M1, and M2 subtypes in response to external stimuli (M-CSF, IFN-γ and LPS, and IL4, respectively) *via* membrane expression of M1 markers CD80 and CD86 and M2 markers CD36 and CD206. Despite different isolation strategies, all M1 MDMs exhibited elevated membrane expression of CD80 and CD86, as expected. Likewise, isolation strategy also did not influence M2 MDM expression levels of CD36 and CD206, which were both increased, as expected (Fig. 3A). Nielsen *et al.* also showed negligible differences between monocytes isolated from positive and negative

Open Access Article. Published on 27 October 2025. Downloaded on 4/18/2026 8:16:51 AM.
This article is licensed under a Creative Commons Attribution-NonCommercial 3.0 Unported Licence.

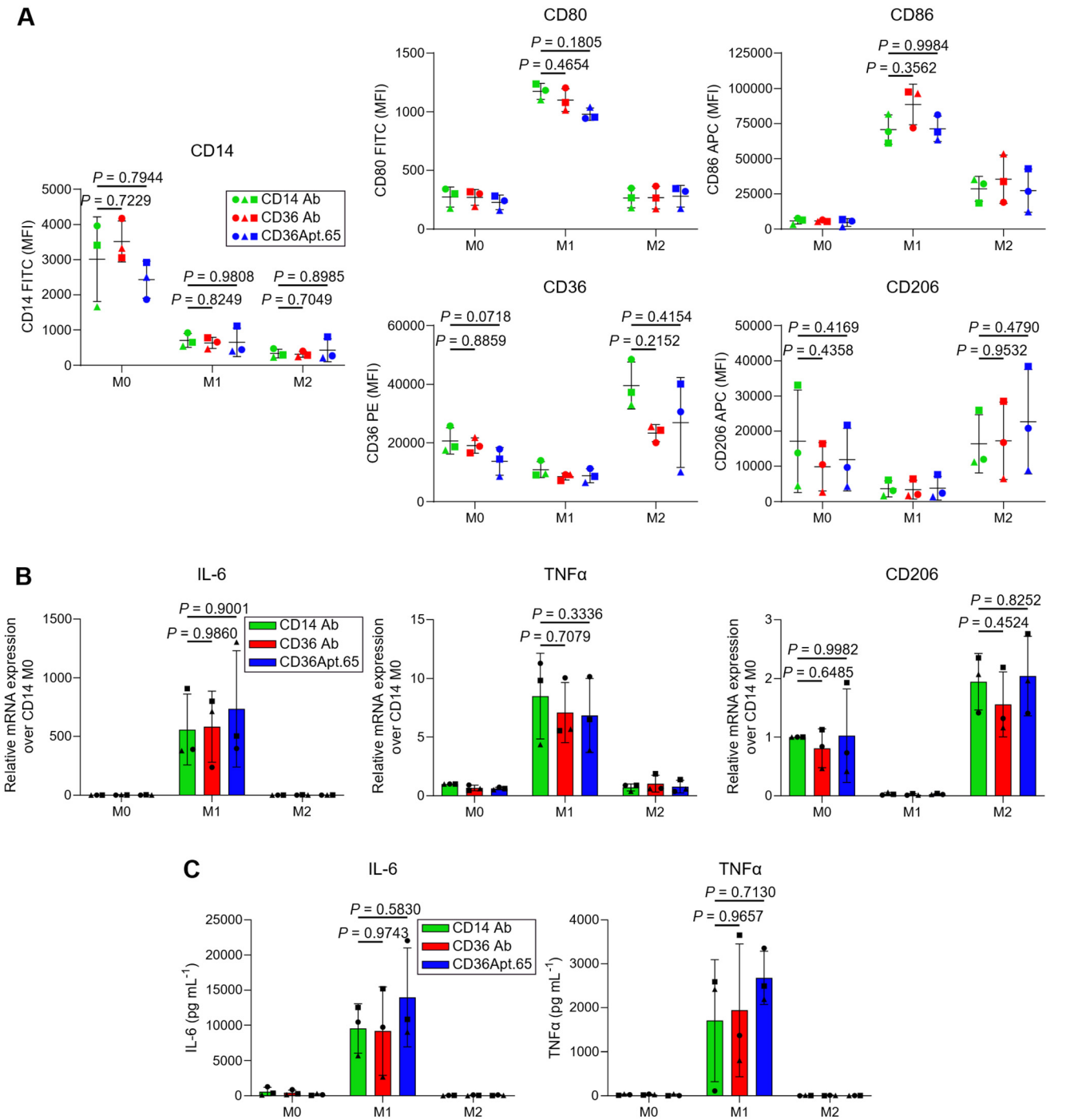


**Fig. 3** Characterization of monocyte-derived macrophages (MDMs) generated from CD14 Ab, CD36 Ab, and CD36Apt.65 aptamer-isolated cells. (A) Flow cytometry surface marker expression levels of CD14, CD80, CD86, CD36, and CD206 from M0, M1, and M2 MDMs from the three different isolation strategies. (B) Gene expression profiles of IL-6, TNFα, and CD206 in M0, M1, and M2 MDMs from the three different isolation strategies normalized to household gene GAPDH. Relative expression levels were adjusted over CD14-isolated M0 MDMs. (C) Soluble cytokine production of IL-6 and TNFα from M0, M1, and M2 MDMs from the three different isolation strategies. Cytokine release as measured using the LEGENDplex assay from BioLegend. Circles, squares, and triangles correspond to different donors, of which experiments were performed in technical triplicates. Horizontal lines/bars and error bars represent the mean and s.d.; $n = 3$; $P > 0.5$ (two-way ANOVA).

selection in CD80 and CD206 membrane expression levels, in agreement with our results.[13] Both aptamer-based selection and negative selection result in unlabeled monocytes, making this comparison practical. Next, we evaluated MDM phenotypes by gene expression of pro-inflammatory M1 genes IL-6 and TNFα, and M2 gene CD206. The isolation method did not affect the genetic profile of M1 MDMs, as all M1 MDMs showed the expected increase in IL6 and TNFα mRNA


This journal is © The Royal Society of Chemistry 2025

Open Access Article. Published on 27 October 2025. Downloaded on 4/18/2026 8:16:51 AM. This article is licensed under a Creative Commons Attribution-NonCommercial 3.0 Unported Licence.

expression levels. All M2 MDMs also showed similar elevated levels of CD206 mRNA expression (Fig. 3B), similar to previously reported results.[13] Finally, we collected cell culture supernatants 48 h after polarization to measure the cytokine release profiles of pro-inflammatory cytokines IL-6 and TNFα. Regardless of isolation method, all M1 MDMs secreted similar elevated levels of both pro-inflammatory cytokines (Fig. 3C). Interestingly, Nielsen *et al.* demonstrated higher levels of pro-inflammatory cytokine secretion in monocytes isolated *via* positive selection compared to those isolated *via* negative selection.[13] This could be due to the lower purity of negative selection and increased contamination with $CD14^-$ leukocytes.

In summary, all three isolation methods (CD14 Ab, CD36 Ab, and CD36Apt.65 aptamer) resulted in MDMs that (1) polarized appropriately in response to M1 and M2 stimuli based on surface marker and gene expression profiles and (2) demonstrated appropriate functional activity, based on cytokine secretion levels.

## 4. Conclusions

Here, we present a novel CD36 aptamer-mediated magnetic bead cell selection strategy to isolate monocytes from PBMCs with high purity and yield. We robustly achieved high purity (89.8%) and yield (74.8%) for several PBMC donors using this platform. With a complementary reversal agent that elutes untouched monocytes, we observed higher preservation of CD14 and CD36 expression in monocytes from aptamer-mediated isolation compared to those from CD14 and CD36 antibody-mediated isolation, respectively. This will likely reduce monocyte activation risks for applications in monocyte-derived therapies. Monocytes isolated by our CD36 aptamer approach showed higher phagocytic potential than those isolated from CD14 Ab, suggesting better immune function *via* unlabeled monocytes. Monocytes from the three different isolation techniques did not exhibit any difference in TLR agonist inflammatory responses. Macrophages derived from isolated monocytes from the antibody and aptamer strategies did not exhibit any significant differences in M1 or M2 polarization, thus suggesting proper phenotypic and functional properties.

Aptamers for cell isolation prove to be an attractive alternative due to reduced cost of cell separations, decreased immunogenicity and cell activation risk, and traceless, reversal agent elution. Reversal agent elution can also allow for multiple, sequential cell selections within the same column, thus increasing efficiency of cell separation and reducing cost and labor.

## Author contributions

M. L. designed the experiments, analyzed results, and prepared the manuscript. A. W. and N. K. helped with aptamer receptor identification and analysis. M. N. and J. A. H. helped with monocyte phagocytosis and TLR agonist response assays. S. H. P. acquired funding in support of the work and supervised the project. All authors reviewed and edited the manuscript.

## Conflicts of interest

There are no conflicts of interest to declare.

## Data availability

Data from this article is available at Mendeley Data, V1, https://doi.org/10.17632/mbzxtvg63s.1. Supplementary information (SI) is available. See DOI: https://doi.org/10.1039/d5bm01232e.

## Acknowledgements

This work was supported by the National Institute of Biomedical Imaging and Bioengineering of the National Institutes of Health (1R01EB034235). The mass spectrometry work was supported by NIH P30 CA015704 of the Fred Hutch/University of Washington/Seattle Children's Cancer Consortium, which includes the Proteomics and Metabolomics Shared Resource (RRID: SCR_022618). M. L. was supported by a National Science Foundation Graduate Research Fellowship under grant no. DGE-214004. We are grateful to J. Zalatan for allowing use of the ForteBio Octet Red96 instrument for BLI experiments, and to M. Davison for use of the CD36 plasmid.

## References

1 Z. A. Cohn, *Adv. Immunol.*, 1968, **9**, 163–214.
2 K. Santa, *Macrophages: Phagocytosis, Antigen Presentation, and Activation of Immunity* (Book Section), 2023, DOI: 10.5772/intechopen.110832.
3 R. M. Steinman and H. Hemmi, in *From Innate Immunity to Immunological Memory*, Springer Berlin Heidelberg, 2006, vol. 311, pp. 17–58.
4 D. Bhatia, R. Dolcetti and R. Mazzieri, *J. Exp. Clin. Cancer Res.*, 2025, **44**, 98.
5 F. Sabir, R. K. Farooq, A. U. Rehman and N. Ahmed, *Curr. Pharm. Des.*, 2019, **24**, 5296–5312.
6 D. Aldarondo and E. Wayne, *Adv. Drug Delivery Rev.*, 2022, **182**, 114116.
7 E. L. Hopewell and C. Cox, *Mol Ther Methods Clin Dev.*, 2020, **16**, 155–160.
8 E. Anassi and U. A. Ndefo, *Pharm. Ther.*, 2011, **36**, 197–202.
9 M. Klichinsky, M. Ruella, O. Shestova, X. M. Lu, A. Best, M. Zeeman, M. Schmierer, K. Gabrusiewicz, N. R. Anderson, N. E. Petty, K. D. Cummins, F. Shen, X. Shan, K. Veliz, K. Blouch, Y. Yashiro-Ohtani, S. S. Kenderian, M. Y. Kim, R. S. O'Connor, S. R. Wallace, M. S. Kozlowski, D. M. Marchione, M. Shestov, B. A. Garcia, C. H. June and S. Gill, *Nat. Biotechnol.*, 2020, **38**(8), 947–953.
10 K. Hadiloo, S. Taremi, M. Heidari and A. Esmaeilzadeh, *Biomarker Res.*, 2023, **11**, 103.
11 D. Zucker-Franklin, *J. Immunol.*, 1974, **112**, 234–240.

Open Access Article. Published on 27 October 2025. Downloaded on 4/18/2026 8:16:51 AM. This article is licensed under a Creative Commons Attribution-NonCommercial 3.0 Unported Licence.

12 R. van Furth, J. A. Raeburn and T. L. van Zwet, *Blood*, 1979, **54**, 485–500.
13 M. C. Nielsen, M. N. Andersen and H. J. Møller, *Immunology*, 2020, **159**, 63–74.
14 M. Meskini, A. Amanzadeh, F. Salehi, S. Bouzari, M. Karimipoor, A. Fuso, A. Fateh and S. D. Siadat, *Sci. Rep.*, 2024, **14**, 23956.
15 S. Haskill, C. Johnson, D. Eierman, S. Becker and K. Warren, *J. Immunol.*, 1988, **140**, 1690–1694.
16 A. M. Dohnal, S. Graffi, V. Witt, C. Eichstill, D. Wagner, S. Ul-Haq, D. Wimmer and T. Felzmann, *J. Cell. Mol. Med.*, 2009, **13**, 125–135.
17 M. Eyrich, S. C. Schreiber, J. Rachor, J. Krauss, F. Pauwels, J. Hain, M. Wölfl, M. B. Lutz, S. de Vleeschouwer, P. G. Schlegel and S. W. Van Gool, *Cytotherapy*, 2014, **16**, 946–964.
18 V. Pullarkat, R. Lau, S.-M. Lee, J. G. Bender and J. S. Weber, *J. Immunol. Methods*, 2002, **267**, 173–183.
19 T. Felzmann, V. Witt, D. Wimmer, G. Ressmann, D. Wagner, P. Paul, K. Hiittner and G. Fritsch, *Cytotherapy*, 2003, **5**, 391–398.
20 Z. Wu, Z. Zhang, Z. Lei and P. Lei, *Cytokine Growth Factor Rev.*, 2019, **48**, 24–31.
21 E. L. Cheng, N. Kacherovsky and S. H. Pun, *ACS Appl. Mater. Interfaces*, 2022, **14**, 44136–44146.
22 N. Kacherovsky, I. I. Cardle, E. L. Cheng, J. L. Yu, M. L. Baldwin, S. J. Salipante, M. C. Jensen and S. H. Pun, *Nat. Biomed. Eng.*, 2019, **3**, 783.
23 B. P. Gray, M. D. Requena, M. D. Nichols and B. A. Sullenger, *Cell Chem. Biol.*, 2020, **27**, 232–244.e7.
24 M. Labib, B. Green, R. M. Mohamadi, A. Mepham, S. U. Ahmed, L. Mahmoudian, I.-H. Chang, E. H. Sargent and S. O. Kelley, *J. Am. Chem. Soc.*, 2016, **138**, 2476–2479.
25 W. Sheng, T. Chen, R. Kamath, X. Xiong, W. Tan and Z. H. Fan, *Anal. Chem.*, 2012, **84**, 4199–4206.
26 L. F. Yang, M. Ling, N. Kacherovsky and S. H. Pun, *Chem. Sci.*, 2023, **14**, 4961–4978.
27 M. R. Dunn, R. M. Jimenez and J. C. Chaput, *Nat. Rev. Chem.*, 2017, **1**, 0076.
28 S. Kosuri and G. M. Church, *Nat. Methods*, 2014, **11**, 499–507.
29 J. Muslehiddinoglu, R. Simler, M. L. Hill, C. Mueller, J. H. A. Amery, L. Dixon, A. Watson, K. Storch, C. Gazziola, F. Gielen, S. A. Lange, J. D. Prail and D. P. Nesta, *Nucleic Acid Ther.*, 2020, **30**, 189–197.
30 J. Zhou and J. Rossi, *Nat. Rev. Drug Discovery*, 2017, **16**, 181–202.
31 K. R. Six, S. Vertongen, S. Seghers, D. De Bleser, V. Compernolle and H. B. Feys, *J. Immunol. Methods*, 2024, **533**, 113733.
32 E. L. Cheng, I. I. Cardle, N. Kacherovsky, H. Bansia, T. Wang, Y. Zhou, J. Raman, A. Yen, D. Gutierrez, S. J. Salipante, A. Des Georges, M. C. Jensen and S. H. Pun, *J. Am. Chem. Soc.*, 2022, **144**, 13851–13864.
33 M. Sylvestre, C. P. Saxby, N. Kacherovsky, H. Gustafson, S. J. Salipante and S. H. Pun, *Bioconjugate Chem.*, 2020, **31**, 1899–1907.
34 D. Shangguan, Z. Cao, L. Meng, P. Mallikaratchy, K. Sefah, H. Wang, Y. Li and W. Tan, *J. Proteome Res.*, 2008, **7**, 2133–2139.
35 D. Van Simaeys, D. Turek, C. Champanhac, J. Vaizer, K. Sefah, J. Zhen, R. Sutphen and W. Tan, *Anal. Chem.*, 2014, **86**, 4521–4527.
36 M.-S. Woo, J. Yang, C. Beltran and S. Cho, *J. Biol. Chem.*, 2016, **291**, 23654–23661.
37 S. C. May and D. Sahoo, *Ann. Blood*, 2021, **6**, 33–33.
38 R. F. Thorne, C. J. Meldrum, S. J. Harris, D. J. Dorahy, D. R. Shafren, M. C. Berndt, G. F. Burns and P. G. Gibson, *Biochem. Biophys. Res. Commun.*, 1997, **240**, 812–818.
39 L. Daviet, E. Malvoisin, T. F. Wild and J. L. McGregor, *Thromb. Haemostasis*, 1997, **78**, 897–901.
40 H. Gao, F. Volat, L. Sandhow, J. Galitzky, T. Nguyen, D. Esteve, G. Åström, N. Mejhert, S. Ledoux, C. Thalamas, P. Arner, J.-C. Guillemot, H. Qian, M. Rydén and A. Bouloumié, *Stem Cells*, 2017, **35**, 1799–1814.
41 M. A. Talle, P. E. Rao, E. Westberg, N. Allegar, M. Makowski, R. S. Mittler and G. Goldstein, *Cell. Immunol.*, 1983, **78**, 83–99.
42 R. A. Swerlick, K. H. Lee, T. M. Wick and T. J. Lawley, *J. Immunol.*, 1992, **148**, 78–83.
43 A. Ghosh, G. Murugesan, K. Chen, L. Zhang, Q. Wang, M. Febbraio, R. M. Anselmo, K. Marchant, J. Barnard and R. L. Silverstein, *Blood*, 2011, **117**, 6355–6366.
44 F.-L. Hsieh, L. Turner, J. R. Bolla, C. V. Robinson, T. Lavstsen and M. K. Higgins, *Nat. Commun.*, 2016, **7**, 12837.
45 Y. Chen, J. Zhang, W. Cui and R. L. Silverstein, *J. Exp. Med.*, 2022, **219**(6), e20211314.
46 L.-Y. Chu, D. P. Ramakrishnan and R. L. Silverstein, *Blood*, 2013, **122**, 1822–1832.
47 A. S. Asch, J. Barnwell, R. L. Silverstein and R. L. Nachman, *J. Clin. Invest.*, 1987, **79**, 1054–1061.
48 I. N. Baranova, R. Kurlander, A. V. Bocharov, T. G. Vishnyakova, Z. Chen, A. T. Remaley, G. Csako, A. P. Patterson and T. L. Eggerman, *J. Immunol.*, 2008, **181**, 7147–7156.
49 M. Y. Pepino, O. Kuda, D. Samovski and N. A. Abumrad, *Annu. Rev. Nutr.*, 2014, **34**, 281–303.
50 Y. Pu, J. Xiang, X. Zhang, Y. Deng, H. Liu and W. Tan, *Anal. Chem.*, 2021, **93**, 3951–3958.
51 P. Kern, W. Kolowos, M. Hagenhofer, C. Frank, J. R. Kalden and M. Herrmann, *Eur. J. Immunogenet.*, 1999, **26**, 337–342.
52 J. Bhattacharjee, B. Das, A. Mishra, P. Sahay and P. Upadhyay, *F1000Res.*, 2018, **6**, 2045.
53 G. D. Thomas, A. A. J. Hamers, C. Nakao, P. Marcovecchio, A. M. Taylor, C. McSkimming, A. T. Nguyen, C. A. McNamara and C. C. Hedrick, *Arterioscler., Thromb., Vasc. Biol.*, 2017, **37**, 1548–1558.
54 J. G. Lee, K. E. Jaeger, Y. Seki, Y. Wei Lim, C. Cunha, A. Vuchkovska, A. J. Nelson, A. Nikolai, D. Kim, M. Nishimura, K. L. Knight, P. White and M. Iwashima, *Immunology*, 2021, **163**, 293–309.

 This journal is © The Royal Society of Chemistry 2025

Open Access Article. Published on 27 October 2025. Downloaded on 4/18/2026 8:16:51 AM. This article is licensed under a Creative Commons Attribution-NonCommercial 3.0 Unported Licence.

55 M. Moniuszko, K. Kowal, M. Rusak, M. Pietruczuk, M. Dabrowska and A. Bodzenta-Lukaszyk, *Clin. Vaccine Immunol.*, 2006, **13**, 704–707.
56 K. Comella, M. Nakamura, K. Melnik, J. Chosy, M. Zborowski, M. A. Cooper, T. A. Fehniger, M. A. Caligiuri and J. J. Chalmers, *Cytometry*, 2001, **45**, 285–293.
57 M. Ling, I. I. Cardle, K. Song, A. J. Yan, N. Kacherovsky, M. C. Jensen and S. H. Pun, *ACS Biomater. Sci. Eng.*, 2023, **9**, 5062–5071.
58 M. Lönne, S. Bolten, A. Lavrentieva, F. Stahl, T. Scheper and J. G. Walter, *Biotechnol. Rep.*, 2015, **8**, 16.
59 S. Schreier, P. Sawaisorn, R. Udomsangpetch and W. Triampo, *J. Transl. Med.*, 2017, **15**, 6.
60 S. Waseem, M. Allen, S. Schreier, R. Udomsangpetch and S. Bhakdi, *Int. J. Mol. Sci.*, 2014, **15**, 8821–8834.
61 R. Peytavi, L. Tang, F. R. Raymond, K. Boissinot, L. Bissonnette, M. Boissinot, F. J. Picard, A. Huletsky, M. Ouellette and M. G. Bergeron, *BioTechniques*, 2005, **39**, 89–96.
62 J. I. Abdul Rashid, N. A. Yusof, J. Abdullah and R. H. Shomiad Shueb, *RSC Adv.*, 2023, **13**, 18748–18759.
63 W. Qiao, H.-C. Chiang, H. Xie and R. Levicky, *Chem. Commun.*, 2015, **51**, 17245–17248.
64 D. Kim and J. Y. Kim, *Mol. Immunol.*, 2014, **57**, 210–215.
65 C. Neu, A. Sedlag, C. Bayer, S. Förster, P. Crauwels, J.-H. Niess, G. van Zandbergen, G. Frascaroli and C. U. Riedel, *PLoS One*, 2013, **8**, e66898.
66 A. Etzerodt, M. B. Maniecki, K. Møller, H. J. Møller and S. K. Moestrup, *J. Leukocyte Biol.*, 2010, **88**, 1201–1205.
67 T. S. Kapellos, L. Bonaguro, I. Gemünd, N. Reusch, A. Saglam, E. R. Hinkley and J. L. Schultze, *Front. Immunol.*, 2019, **10**, 2035.
68 P. Sampath, K. Moideen, U. D. Ranganathan and R. Bethunaickan, *Front. Immunol.*, 2018, **9**, 1726.
69 K. Colleselli, A. Stierschneider and C. Wiesner, *Int. J. Mol. Sci.*, 2023, **24**, 12464.
70 A. Ozinsky, D. M. Underhill, J. D. Fontenot, A. M. Hajjar, K. D. Smith, C. B. Wilson, L. Schroeder and A. Aderem, *Proc. Natl. Acad. Sci. U. S. A.*, 2000, **97**, 13766–13771.
71 Y. Wang, Y. Zhou, H. Fang, S. Lin, P. Wang, R. Xiong, J. Chen, X. Xiong, F. Lv, Q. Liang and Q. Yang, *Ann. Neurol.*, 2014, **75**, 876–889.
72 S. Su, L. Tao, Z. Deng, W. Chen, S. Qin and H. Jiang, *Scand. J. Immunol.*, 2021, **93**(4), e12988.
73 A.-C. Raby, B. Holst, E. Le Bouder, C. Diaz, E. Ferran, L. Conraux, J.-C. Guillemot, B. Coles, A. Kift-Morgan, C. S. Colmont, T. Szakmany, P. Ferrara, J. E. Hall, N. Topley and M. O. Labéta, *Sci. Transl. Med.*, 2013, **5**(185), 185ra64.
74 T. Abe, M. Shimamura, K. Jackman, H. Kurinami, J. Anrather, P. Zhou and C. Iadecola, *Stroke*, 2010, **41**, 898–904.
75 H.-J. Kim, H. Kim, J.-H. Lee and C. Hwangbo, *Immun. Ageing*, 2023, **20**, 67.
76 C. M. Paulos, A. Kaiser, C. Wrzesinski, C. S. Hinrichs, L. Cassard, A. Boni, P. Muranski, L. Sanchez-Perez, D. C. Palmer, Z. Yu, P. A. Antony, L. Gattinoni, S. A. Rosenberg and N. P. Restifo, *Clin. Cancer Res.*, 2007, **13**, 5280–5289.
77 A. Ciesielska, M. Matyjek and K. Kwiatkowska, *Cell. Mol. Life Sci.*, 2021, **78**, 1233–1261.
78 S. C. Gangloff, U. Zähringer, C. Blondin, M. Guenounou, J. Silver and S. M. Goyert, *J. Immunol.*, 2005, **175**, 3940–3945.
79 Z. Jiang, P. Georgel, X. Du, L. Shamel, S. Sovath, S. Mudd, M. Huber, C. Kalis, S. Keck, C. Galanos, M. Freudenberg and B. Beutler, *Nat. Immunol.*, 2005, **6**, 565–570.
80 J. A. Philips, E. J. Rubin and N. Perrimon, *Science*, 2005, **309**, 1251–1253.
81 D. Cao, J. Luo, D. Chen, H. Xu, H. Shi, X. Jing and W. Zang, *Sci. Rep.*, 2016, **6**, 23132.
82 C. Yunna, H. Mengru, W. Lei and C. Weidong, *Eur. J. Pharmacol.*, 2020, **877**, 173090.
83 P. Chaintreuil, E. Kerreneur, M. Bourgoin, C. Savy, C. Favreau, G. Robert, A. Jacquel and P. Auberger, *Front. Immunol.*, 2023, **14**, 1178337.
84 Y. Pan, Y. Yu, X. Wang and T. Zhang, *Front. Immunol.*, 2020, **11**, 583084.
85 D. Chen, J. Xie, R. Fiskesund, W. Dong, X. Liang, J. Lv, X. Jin, J. Liu, S. Mo, T. Zhang, F. Cheng, Y. Zhou, H. Zhang, K. Tang, J. Ma, Y. Liu and B. Huang, *Nat. Commun.*, 2018, **9**, 873.
86 H. Bruns, M. Büttner, M. Fabri, D. Mougiakakos, J. T. Bittenbring, M. H. Hoffmann, F. Beier, S. Pasemann, R. Jitschin, A. D. Hofmann, F. Neumann, C. Daniel, A. Maurberger, B. Kempkes, K. Amann, A. Mackensen and A. Gerbitz, *Sci. Transl. Med.*, 2015, **7**(282), 282ra47.
87 C. Ngambenjawong, H. H. Gustafson and S. H. Pun, *Adv. Drug Delivery Rev.*, 2017, **114**, 206–221.
88 S. K. Biswas and A. Mantovani, *Nat. Immunol.*, 2010, **11**, 889–896.
89 A. Sica and A. Mantovani, *J. Clin. Invest.*, 2012, **122**, 787–795.